SONAR Images Despeckling Using a Bayesian Approach in the Wavelet Domain

Sorin Moga*[a], Alexandru Isar[b],
[a] GET / ENST Bretagne, TAMCIC / CNRS UMR 2872, Techople Brest-Iroise, CS 83818 -29238 Brest, Cedex 3 FRANCE;
[b]Dept. of Communications, "Politehnica" Univ. Timisoara, ROMANIA

ABSTRACT

During acquisition, the SONAR images are corrupted by multiplicative noise (speckle).The aim of an image denoising algorithm is then to reduce the noise level, while preserving the image features. There is a great diversity of wavelet based estimators used like denoising systems. The corresponding denoising methods have three steps: the computation of the forward Wavelet Transform (WT); the filtering of the wavelet coefficients; and the computation of the inverse wavelet transform of the result obtained. In the following, the Dual Tree Complex Wavelet Transform (DT-CWT) will be associated with a variant of a maximum a posteriori bishrink filter because its explicit input-output relation permits a sensitivity analysis. The bishrink filter has a high sensitivity with some parameters, especially in the homogeneous regions. The main idea of this paper is to reduce this sensitivity by diversification. In this respect the regions with different homogeneity degrees are identified and in each of them the WT of the acquired image is filtered using a number of different variants of bishrink filters in accordance with its homogeneity.

Keywords: Bishrink filter, estimation, sensitivity, statistical model, SONAR images.

1. Introduction

The SONAR systems are used in a large spectrum of military or civil applications. The user is able to distinguish a number of different regions, analyzing a SONAR image. This classification process is sometimes very difficult, due to the presence of the speckle. The use of anti-speckle filters is required before the application of a detection or classification procedure. Such a filter must realize an important speckle reduction in the regions where the sonar reflectivity is constant and a conservation of the textures and other structures of the seafloor image in the other regions. Some classical estimators are: the Kuan's filter (linear estimator which minimizes the mean squared estimation error) and the Frost's filter (Wiener filter matched to multiplicative noise). The signal to noise ratio (SNR) of those images can be very small, depending on their acquisition conditions. They contain large homogeneous regions. The majority of algorithms founded in literature do not refer to this kind of images. The SONAR images are a particular case of Synthetic Aperture Radar (SAR) images. The speckle that perturbs the SAR images is a white noise distributed following a law Gamma, which parameter is the number of views, L: $p_{X_\Gamma}(x) = \frac{L^L}{\Gamma(L)} \cdot x^{L-1} \cdot e^{-Lx}$ for $x \geq 0$, where Γ represents the Euler's Gamma function. Its mean is given by: $\mu_\Gamma = 1,$ and its variance by: $\sigma_\Gamma^2 = E\left[X_\Gamma^2\right] - \mu_\Gamma^2 = \frac{L(L+1)}{L^2} - 1 = \frac{1}{L}.$

The problem of denoising SAR images is well analyzed in literature. Some of the best papers on this subject are [1-4]. The speckle noise that perturbs the SONAR images is of multiplicative type. It can be transformed into an additive noise with the aid of a logarithm computation block. The random variable X_Γ is transformed obtaining the random variable $Y_{\log-\Gamma}$, which describes the speckle noise at the input of the second block, in accordance with the change of variable realized by the first block in figure 1. The relation between the probability density functions, (pdf), of these two random variables is:

$$p_{Y_{\log-\Gamma}}(y)=\left.\frac{p_{X_\Gamma}(x)}{\left|\frac{dy}{dx}\right|}\right|_{x=e^y}=\left.\frac{\frac{L^L}{\Gamma(L)}x^{L-1}e^{-Lx}}{\frac{1}{x}}\right|_{x=e^y}=\left.\frac{L^L}{\Gamma(L)}x^L e^{-Lx}\right|_{x=e^y}=\frac{L^L}{\Gamma(L)}e^{Ly}e^{-Le^y}.$$

The value of the mean of the law log-Gamma is given by: $\mu_{\log-\Gamma}=\sum_{k=1}^{L-1}\frac{1}{k}-\gamma-\ln L$, where γ represents the Euler's number. Its variance is: $\sigma^2_{\log-\Gamma}=\frac{\pi^2}{6}-\sum_{k=1}^{L-1}\frac{1}{k^2}$. So, the noise that perturbs the logarithm of the useful part of the SAR image is white and distributed following a law log-Gamma. At the end, to obtain the denoising result the logarithm inversion must be performed. The denoising system must contain a mean correction block also. The architecture of the proposed denoising system is presented in figure 1. For the design of the denoising kernel there are multiple solutions. Natural images are often corrupted by additive noise that can be modeled as Gaussian. The multiresolution analysis performed by the wavelet transform is a powerful tool to achieve these goals. In the wavelet domain, the noise is uniformly spread throughout the coefficients, while most of the image information is concentrated in the few largest ones (sparsity of the wavelet representation). The most straightforward way of distinguishing information from noise in the wavelet domain consists of thresholding the wavelet coefficients. Soft-thresholding is the most popular thresholding strategy and has been theoretically justified by Donoho and Johnstone, [5]. These authors propose a three steps denoising algorithm: 1. the computation of a forward WT, 2. the filtering with a non-linear filter, 3. the computation of the corresponding inverse wavelet transform (IWT). They use the Discrete Wavelet Transform (DWT) and the soft-thresholding filter. Their unique statistical hypothesis refers to the noise, considered additive white and Gaussian, (AWGN). The soft–thresholding filter puts to zero all the wavelet coefficients with the absolute value smaller then a threshold. This threshold is selected to minimize the min-max approximation error. The soft-thresholding filter was enhanced in [6], where the same hypotheses concerning the clean image and the noise were considered. The approach proposed in [6] consists in parametrizing the denoising method (by linear combination of nonlinear thresholding functions) and choosing the parameters that minimize the mean square approximation error, (MSE). The WT used in [6] was also the DWT. Generally, the denoising results reported in [6] are very good but they are sensitive with the statistical content of the clean image (for example the results obtained for the image Peppers are much better then the results obtained for the image Barbara). The soft-thresholding filter is used in [2] for the denoising of SAR images in association with a complex WT. Some relatively recent research has addressed the development of statistical models of wavelet coefficients of natural images and application of those models to image denoising. Highly effective yet simple schemes mostly based on soft thresholding have been developed [7, 8]. An appealing particularity of the WTs is the inter-scale dependence. If at a given scale a coefficient is large, its correspondent at the next scale (having the same spatial coordinates) will be also large. In [6], [7] and [8] the inter-scale dependencies are used to improve the denoising performance. The wavelet coefficients statistical models which exploit the dependence between coefficients give better results compared to the ones using an independent assumption [9, 10], [12, 13]. The denoising is performed in [9] and [10] with the aid of maximum a posteriori filters, (MAP). If we denote with *w* the wavelet coefficients of the clean image and with *n* the wavelet coefficients of the noise then it can be written, $y=w+n$. The MAP estimation of w, $\hat{w}$, realized using the observation *y* is given by the following MAP filter equation: $\hat{w}=\arg\max_w\{\log(p_n(y-w)p_w(w))\}$, where p_x represents the pdf of *x*. Generally, the last equation has not analytical solution. There are some exceptions. If both *w* and *n* are Gaussian distributed, $p_w(w)=\frac{1}{\sqrt{2\pi}\sigma}\cdot e^{-\frac{w^2}{2\sigma^2}}$; $p_n(n)=\frac{1}{\sqrt{2\pi}\sigma_n}\cdot e^{-\frac{n^2}{2\sigma_n^2}}$, then the MAP filter becomes the very well known zero order Wiener filter. Its input-output relation (the solution of the MAP filter equation) is: $\hat{w}=\frac{\sigma^2}{\sigma^2+\sigma_n^2}y$. To apply this relation, the two variances must be estimated. Generally, the noise variance is estimated globally using the diagonal sub-image obtained at the first wavelet decomposition level (named HH sub-image in the case of the DWT) with the aid of a median estimator, [5]. The precision of the estimation given in the last relation can be improved if a

local estimation of the standard deviation of the clean image is considered, $(\sigma \to \hat{\sigma}_l)$. This local standard deviation can be estimated in a moving window centered in the current pixel. Generally it is a rectangular window. If the coordinates of the current pixel are (*i*,*j*) then the input-output relation of the local zero order Wiener filter is given by: $\hat{w}(i,j) = \frac{\hat{\sigma}_l^{\,2}(i,j)}{\hat{\sigma}_l^{\,2}(i,j) + \hat{\sigma}_n^2}\, y$. The model of naturally images is given by heavy tailed distributions, [9]. So, the utilization of zero-order Wiener filters in image denoising applications can not furnish the best performance. This drawback is partially compensated by a better estimation of the local variance of the clean image, realized with the aid of two-stage denoising system. The first stage treats the acquired image furnishing a pilot for the second stage. The acquired image is once again treated by the second stage but this time the information carried by the pilot is used. The idea of two-stage denoising systems was introduced in [14] in the context of one dimension signals. The first stage of the algorithm in [14] is a denoising system that utilizes the hard-thresholding filter, [5], in the field of DWT. The role of the pilot signal is to permit the improvement of the clean signals' variance estimation required in the second stage of the denoising algorithm. This second stage associates another DWT (computed with the aid of other mother wavelets) with a zero order Wiener filter. Other two-stage denoising algorithms applied to images were proposed in [15, 16]. A very nice contribution of [16] is the idea of directional windows. The rectangular windows used for the estimation of the local variance of the clean image are replaced by elliptical windows oriented following the preferential direction of the current detail sub-image. So, in the case of the DWT the principal axes of the elliptical windows make an angle with the horizontal direction of 0° for the horizontal detail sub-images, of ± 45° for the diagonal detail sub-images and of 90° for the vertical detail sub-images. This is a first example of exploiting the intra-scale dependence of the wavelet coefficients, mentioned in [6]. If *n* is Gaussian distributed and *w* has a Laplacian distribution (this is a heavy tailed one) then the MAP filter becomes an adaptive soft thresholding filter. In this case: $p_w(w) = \frac{1}{\sqrt{2}\sigma} \cdot e^{-\frac{\sqrt{2}|w|}{\sigma}}$; $p_n(n) = \frac{1}{\sqrt{2\pi}\sigma_n} \cdot e^{-\frac{n^2}{2\sigma_n^2}}$. The MAP filter equation's solution becomes: $\hat{w} = \mathrm{sgn}(y)\left(|y| - \sqrt{2}\,\frac{\sigma_n^2}{\sigma}\right)_+$, where: $(X)_+ = \begin{cases} X & \text{for} \quad X > 0 \\ 0 & \text{otherwise} \end{cases}$. This is a soft-thresholding filter with threshold value $\sqrt{2}\,\frac{\sigma_n^2}{\sigma}$. Once again the two standard deviations must be estimated. The local variant of this MAP filter is described by: $\hat{w}(i,j) = \mathrm{sgn}(y(i,j))\left(|y(i,j)| - \sqrt{2}\,\frac{\hat{\sigma}_n^2}{\hat{\sigma}(i,j)}\right)_+$. The zero order Wiener filter and the adaptive soft-thresholding filter are two examples of marginal MAP filters. If the models of the clean image and of the noise are bivariate distributions then the MAP filter can take into account the inter-scale dependence of the wavelet coefficients. This is the case of the bishrink filter, [9], that represents the subject of this paper. In this case the coefficient w_2 represents the parent of the coefficient w_1 (w_2 is the wavelet coefficient at the same position as w_1, but at the next coarser scale). Then: $y_k = w_k + n_k$, $k = 1,2$ and the vectors $\boldsymbol{w} = (w_1, w_2)$, $\boldsymbol{y} = (y_1, y_2)$ and $\boldsymbol{n} = (n_1, n_2)$ can be constructed**.** With their aid it can be written: ***y=w+n.*** The noise is assumed i.i.d. Gaussian, $p_{\boldsymbol{n}}(\boldsymbol{n}) = \frac{1}{2\pi\sigma_n^2} \cdot e^{-\frac{n_1^2 + n_2^2}{2\sigma_n^2}}$. The model of the clean image proposed in [9] is:

$$p_{\boldsymbol{w}}(\boldsymbol{w}) = \frac{3}{2\pi\sigma^2} \cdot e^{-\frac{\sqrt{3}}{\sigma}\sqrt{w_1^2 + w_2^2}}. \tag{1}$$

another heavy tailed distribution. The input-output relation of the bishrink filter is:

$$\hat{w}_1 = \frac{\left(\sqrt{y_1^2 + y_2^2} - \frac{\sqrt{3}\sigma_n^2}{\sigma}\right)_+}{\sqrt{y_1^2 + y_2^2}}\, y_1. \tag{2}$$

This estimator requires the prior knowledge of the noise variance and of the marginal variance of the clean image for each wavelet coefficient. To estimate the noise variance from the noisy wavelet coefficients, a robust median estimator is used from the finest scale wavelet coefficients, [5]:

$$\hat{\sigma}_n^2 = \frac{median\left(|y_i|\right)}{0.6745}, \quad y_i \in subband\ \ HH. \tag{3}$$

In [9] the marginal variance of the k^{th} coefficient is estimated using neighboring coefficients in the region $N(k)$, a squared shaped window centered on this coefficient with size 7x7. To make this estimation one gets $\sigma_y^2 = \sigma^2 + \sigma_n^2$ where σ_y^2 represents the marginal variance of noisy observations y_1 and y_2. For the estimation of the marginal variance of noisy observations, in [9] is proposed the following relation:

$$\hat{\sigma}_y^2 = \frac{1}{M} \sum_{y_i \in N(k)} y_i^2, \tag{4}$$

where M is the size of the neighborhood $N(k)$. Then σ can be estimated as:

$$\hat{\sigma} = \sqrt{\left(\hat{\sigma}_y^2 - \hat{\sigma}_n^2\right)_+}. \tag{5}$$

In [10] a similar technique is used but the bivariate a priori pdf of the clean image is considered of SαS type. The distribution of the wavelet coefficients evolves with the increasing of the decomposition level. This model's mobility can be captured if an entire class of distributions is considered. Such a class is characterized with some parameters. For different values of parameters different members of the class are obtained. An example of class of distributions is the SαS family. It contains the Gauss' and Laplace's distributions as elements. The majority of the elements of this family lack a compact analytical expression for their pdf. Such a distribution is most conveniently represented by its characteristic function: $\varphi(\omega) = e^{j\delta\omega - \gamma|\omega|^\alpha}$, where α is the characteristic exponent, taking values $0 < \alpha \le 2$, δ is the location parameter and γ, $(\gamma > 0)$ is the dispersion of the distribution. Using this family of distributions a better model of the clean image (than that used in the case of bishrink filter) at each decomposition level is obtained. Unfortunately in this case the MAP filter equation can not be solved analytically, some numerical methods being required. The advantage of an analytical solution of the MAP filter equation lies in a fast implementation (the numerical methods are avoided) and in the possibility to perform a sensitivity analysis. The WT associated with the MAP filters described in [9] and [10] is no longer the DWT, because it has some drawbacks, [11], the lack of shift invariance, the lack of symmetry of the mother wavelets and the poor directional selectivity. These disadvantages can be diminished using a complex wavelet transform, like for example the DT-CWT, [11]. So, the MAP filters constructed in [9] and [10] act in the field of the DT-CWT. The family of Pearson's distributions was used in **[**4**]** for the construction of MAP filters which associated with the UDWT was used for the denoising of SAR images. Like in [6], the problem of intra-scale dependence of wavelet coefficients is postponed by the authors of [9, 10] and **[**4**]** for future work. The MAP filters can be also used in the spatial domain for the denoising of SAR images, [7]. Taking into account the intra-scale dependence of wavelet coefficients the denoising results can be improved. In [12] is described a method for removing noise from digital images, based on a statistical model of the coefficients of overcomplete multiscale oriented basis. This decomposition is named steerable pyramid. Following it, the image is subdivided into subbands using filters that are polar-separable in the Fourier domain. In scale, the subbands have octave bandwidth with a functional form constrained by a recursive system diagram. In orientation, the functional form is chosen so that the set filters at a given scale span a rotation-invariant subspace. This decomposition can be considered as a WT with shift invariance and very good directional selectivity. Neighborhoods of coefficients at adjacent positions (intra-scale dependence) and scales (inter-scale dependence) are modeled as the product of two independent random variables: a Gaussian vector and a hidden positive scalar multiplier. The latter modulates the local variance of the coefficients in the neighborhood, and is thus able to account for the empirically observed correlation between the coefficients amplitudes. Under this model, named Gaussian scale mixture (GSM), the Bayesian least squares estimate, (BLS) of each coefficient reduces to a weighted average of the local linear estimate over all possible values of the hidden multiplier variable. In [12] is demonstrated through simulations with images contaminated by AWGN that the performance of this method (BLS-GSM) substantially surpasses that of previously published methods, both visually and in terms of mean squared error. In [13] three novel wavelet domain denoising methods for subband-adaptive, spatially-adaptive and multivalued image denoising are developed. The core of this approach is the estimation of the probability that a given coefficient contains a significant noise-free component, which is called signal of interest. In this respect, in [13] are analyzed three cases: (i) signal of interest with fixed amount per subband, (ii) signal of interest conditioned on a

local spatial context (intra-scale dependence) and (iii) signal of interest conditioned on information from multiple image bands (intra-scale and inter-scale dependencies). All these probabilities are estimated assuming a generalized Laplacian prior for clean subband data and additive white Gaussian noise. The results demonstrate that the new subband adaptive shrinkage function outperforms Bayesian thresholding approaches in terms of MSE. The spatially adaptive version of the proposed method yields better results than the existing spatially adaptive ones of similar and higher complexity. The WTs used in [13] are the DWT and the UDWT.

The aim of this paper is to correct the comportment of the bishrink filter in the homogeneous regions of very noisy images. First we prove that the performance of the bishrink filter degrades with the increasing of σ_n and with the decreasing of σ. With the increasing of σ_n the image becomes noisier. The local value of σ measures the degree of homogeneity of the considered region. If, for all the pixels of a given region, $\sigma = 0$, those pixels have the same value. So this is a perfect homogeneous region. Next we propose a new strategy for the correction of those degradations. It is based on architecture in two-stage. In the first stage the genuine denoising algorithm proposed in [9] is applied obtaining the first result. Computing the standard deviation of each pixel of the first result the pilot image is obtained. Its pixels are classified in six regions following their values. The coordinates of the pixels belonging at each of these regions will represent the six masks used in the second stage. At the basis of the construction of the second stage lies the idea of diversification.

The structure of this paper is the following. In the second paragraph is presented a sensitivity analysis of the bishrink filter and some of its drawbacks are identified. Then a solution to reduce these drawbacks is proposed and analyzed. In the third paragraph are given all the details of the proposed denoising algorithm. The fourth paragraph is dedicated to the presentation of the simulation results and to some comparisons with the best available wavelet based image denoising results conceived to illustrate the effectiveness of the proposed algorithm. Two types of simulation are reported, referring to the denoising kernel and to entire denoising system. For the first type of simulation are used general images and for the second type are used SONAR images. The fifth paragraph is dedicated to the paper's conclusion.

2. THE BISHRINK FILTER

The estimator described by (1)-(5) is named bishrink filter and is applied in the field of the DT-CWT. It is a non-linear filter. Currently the design of linear filters is based on sensitivity analyses. This kind of analysis can be generalized in the case of non-linear filters. For example the sensitivity of the bishrink filter with the estimation of the noise standard deviation can be computed with the relation:

$$S_{\hat{w}_1}^{\hat{\sigma}_n} = \frac{d\hat{w}_1}{d\hat{\sigma}_n} \cdot \frac{\hat{\sigma}_n}{\hat{w}_1}. \tag{6}$$

The input-output relation of the bishrink filter (2) can be put in the following form:

$$\hat{w}_1 = \begin{cases} \dfrac{\sqrt{y_1^2 + y_2^2} - \dfrac{\sqrt{3}\hat{\sigma}_n^2}{\hat{\sigma}}}{\sqrt{y_1^2 + y_2^2}} y_1, & \text{if } \sqrt{y_1^2 + y_2^2} > \dfrac{\sqrt{3}\hat{\sigma}_n^2}{\hat{\sigma}}. \\ 0, & \text{in rest} \end{cases} \tag{7}$$

The derivative of the estimation with the estimation of the noise standard deviation becomes:

$$\frac{d\hat{w}_1}{d\hat{\sigma}_n} = \begin{cases} \dfrac{-2\sqrt{3}\hat{\sigma}_n y_1}{\hat{\sigma}\sqrt{y_1^2 + y_2^2}}, & \text{if } \sqrt{y_1^2 + y_2^2} > \dfrac{\sqrt{3}\hat{\sigma}_n^2}{\hat{\sigma}} \\ 0, & \text{in rest} \end{cases}. \tag{8}$$

A sensitivity of estimation with a parameter quantifies the variation of the estimation for a given variation of the parameter. In the case, $\sqrt{y_1^2 + y_2^2} \le \frac{\sqrt{3}\hat{\sigma}_n^2}{\hat{\sigma}}$, our estimation has the value 0 for any variation of the estimation of the noise standard deviation. So, using the last relation, the sensitivity definition and the input-output relation of the bishrink filter, it can be written:

$$S_{\hat{w}_1}^{\hat{\sigma}_n} = \begin{cases} \dfrac{-2\sqrt{3}\hat{\sigma}_n^2}{\hat{\sigma}\sqrt{y_1^2+y_2^2}-\sqrt{3}\hat{\sigma}_n^2}, & \text{if } \sqrt{y_1^2+y_2^2} > \dfrac{\sqrt{3}\hat{\sigma}_n^2}{\hat{\sigma}} \\ 0, & \text{in rest} \end{cases}. \tag{9}$$

The absolute value of this sensitivity is an increasing function of the estimation of the noise standard deviation. When the estimation of the noise standard deviation is higher the performance of the bishrink filter is poorer. One of the goals of this paper is to correct this comportment. Another very important parameter of the bishrink filter is the local estimation of the marginal variance of the clean image, $\hat{\sigma}$. Following a similar derivation, the sensitivity of the estimation $\hat{w}_1$ with $\hat{\sigma}$ is given by:

$$S_{\hat{w}_1}^{\hat{\sigma}} = \begin{cases} \dfrac{\sqrt{3}\hat{\sigma}_n^2}{\hat{\sigma}\sqrt{y_1^2+y_2^2}-\sqrt{3}\hat{\sigma}_n^2}, & \text{if } \sqrt{y_1^2+y_2^2} > \dfrac{\sqrt{3}\hat{\sigma}_n^2}{\hat{\sigma}} \\ 0, & \text{in rest} \end{cases}. \tag{10}$$

This is a decreasing function of $\hat{\sigma}$. The precision of the estimation based on the use of the bishrink filter decreases with the decreasing of $\hat{\sigma}$. So, the bishrink filter treats very well the contours regions of the clean image, the estimation of its textured regions must be corrected and the worst treatment corresponds to its homogeneous regions. The denoising quality of pixels with slightly different σ will be very different in the homogeneous regions. The sensitivity $S_{\hat{w}_1}^{\hat{\sigma}}$ increases with the increasing of $\hat{\sigma}_n$. So, the degradation of the homogeneous and textured zones of the clean image is amplified by the increasing of the noise standard deviation. In consequence the most difficult regime of the bishrink filter corresponds to the treatment of homogeneous regions of very noisy images. The aim of this paper is to reduce the distortion produced by a denoising system based on the DT-CWT and the bishrink filter like a consequence of the sensitivities $S_{\hat{w}_1}^{\hat{\sigma}_n}$ and $S_{\hat{w}_1}^{\hat{\sigma}}$. To do this task a two stage algorithm is conceived. In the first stage the denoising procedure based on the association of a DT-CWT and the genuine bishrink filter described in [9] is applied. The standard deviation of each pixel of the resulted image is computed applying the relation (4) obtaining the pilot image. This image is segmented in six classes following the values of its pixels. The coordinates of the pixels corresponding at each class are identified and the six masks are generated. In the second stage of the proposed algorithm the acquired image is processed once again using the pilot image already obtained. The solution proposed for the second stage is based on the enhancement of the diversity of the estimation. The idea of diversification comes from the communications field where spatial or temporal diversification techniques are used to add a fixed amount of redundancy to a message, improving the information transmission. Finally the extra data are rejected using a fusion procedure and the message is reconstructed in a form as closed as possible to its original one. The diversification principle was already used in denoising. For example, to reduce the unwanted oscillations near edges, that appear because the DWT is not shift-invariant, Coifman and Donoho introduced the cycle-spinning concept, [17]. Rotation invariance can be also obtained using the diversification principle, [18]. This concept was also used in [19] to improve the denoising of SAR and SONAR images. In this paper are proposed three diversification mechanisms. The first one supposes the utilization of two different mother wavelets. The others are based on the utilization of two different variants of bishrink filter, named in the following: adaptive bishrink filter with global estimation of local variance and mixed bishrink filter. Using these diversification mechanisms and the genuine bishrink filter, six estimates, called in the following partial results, are obtained. The final estimate is obtained by the fusion of the six partial results. Inspired by [17-19], we have selected for each of the six classes of the final result the simpler fusion technique, the averaging of some corresponding classes contained in the partial results. Using the six masks obtained at the end of the first stage we identify in each partial result the six corresponding classes. Each one contains only the pixels with the coordinates specified by the corresponding mask. For example all the pixels of the second partial result having the same coordinates like the pixels of the first partial result belonging to the first class will form the first class of the second partial result. This fusion procedure minimizes the MSE of the estimation. The amount of this reduction increases with the number of partial results. So, each of the last five classes of the final result is obtained by averaging the corresponding classes belonging to some partial results. For the sixth class of the final result (corresponding to the homogeneous regions) the corresponding classes of all partial results are averaged. For the fifth class of the final result (the first group of textured regions, having the smaller homogeneity degree) the corresponding classes of only five partial results are averaged and so on. For the second class of the final result (the last group of

textured regions, having the higher homogeneity degree) the corresponding classes of only two partial results are averaged. Finally, for the first class of the final result (corresponding to the contours regions) the corresponding class of a partial result is selected, without averaging. This fusion procedure prevents the oversmoothing. Any of the three variants of the bishrink filter proposed in this paper has better performance then the local zero order Wiener filter. The DT-CWT is superior to the DWT or the UDWT in denoising applications. So, the performance obtained using the proposed denoising method is superior to the performance reported in [15] or in [16].

3. THE SOLUTION PROPOSED

To realize the diversification required in the second stage of the proposed algorithm two types of DT-CWT are computed. Next three variants of bishrink filter are applied in the field of each DT-CWT obtaining six partial results. Averaging the corresponding classes belonging to some partial results the six classes of the final result are obtained. Assembling these classes the final estimation is obtained. The architecture of the proposed denoising system is presented in figure 1. The first stage of the algorithm is represented in red. The second one is represented in blue. Two types of WT, DT-CWT_A and DT-CWT_B are computed obtaining the wavelet coefficients w_A and w_B. Three variants of bishrink filter, F_2–the genuine one, F_1-the bishrink filter with global estimation of the local variance and F_3-the mixed bishrink filter, are applied in the field of each WT. Six estimates of wavelet coefficients $\hat{w}_{1A}$, $\hat{w}_{2A}$, $\hat{w}_{3A}$, $\hat{w}_{1F}$, $\hat{w}_{2F}$ and $\hat{w}_{3F}$, are obtained. For each one is computed the inverse WT, IDT-CWT, obtaining six partial results, $\hat{s}_{1A}$, $\hat{s}_{2A}$, $\hat{s}_{3A}$, $\hat{s}_{1F}$, $\hat{s}_{2F}$ and $\hat{s}_{3F}$. The image $\hat{s}_{2A}$ is segmented in six classes following the values of the local variances of its pixels obtaining the pilot image. Registering the coordinates of the pixels belonging at each of these classes the six masks are generated. With the aid of these masks the six classes of each partial result are identified. Using the class selectors CS_1-CS_6, each partial result is treated in a different manner. The segmentation block, Segm, creates the six masks. Each mask is used by the corresponding CS. These systems pick up the pixels of their input images with the coordinates belonging to the correspondent mask, generating each class of the partial results. CS_1 has only one input and generates with the aid of the sixth mask the first class of the image $\hat{s}_{2A}$. CS_2 has two inputs and generates with the aid of the fifth mask the second classes of the partial results $\hat{s}_{2A}$ and $\hat{s}_{3A}$ and so on. The first class of the final estimate $\hat{s}_1$ is identical with the first class of the image $\hat{s}_{2A}$. The second class of the final result, $\hat{s}_2$, is obtained averaging the pixels belonging to the second classes of the partial results $\hat{s}_{2A}$ and $\hat{s}_{3A}$ and so on. For the last class of the final result, $\hat{s}_6$, containing homogeneous zones, all the pixels belonging to the sixth class of the partial results $\hat{s}_{1A}$, $\hat{s}_{2A}$, $\hat{s}_{3A}$, $\hat{s}_{1F}$, $\hat{s}_{2F}$ and $\hat{s}_{3F}$ are averaged. In the following the construction of each block in figure 1 is presented in detail.

3.1. The Diversification Mechanisms

The first diversification mechanism refers to the construction of the DT-CWT. There are two kinds of filters used for the computation of the DT-CWT: for the first decomposition level and for the other levels, [11]. The diversification is realized by the selection of two types of filters for the first level. The first one is selected from the (9,7)-tap Antonini filters pair and the second one corresponds to the pair of Farras nearly symmetric filters for orthogonal 2-channel perfect reconstruction filter bank, [20]. The other diversification mechanisms refer to the construction of bishrink filter. The filter F_2 is a genuine bishrink filter. The filter F_1 is a bishrink filter with global estimation of the local variance. It was constructed for the reasons presented in the following. The estimation in (5) is not very precise for two reasons. First, it is based on the correct assumption that y_1 and y_2 are modeled as zero mean random variables. But their restrictions to the finite neighborhood $N(k)$ are not necessary zero mean random variables. So, it is better to estimate first the means in the neighborhood:

$$\hat{\mu}_y = \frac{1}{M} \sum_{y_i \in N(k)} y_i, \tag{11}$$

and then the variances:

$$\hat{\sigma}_y^2 = \frac{1}{M} \cdot \sum_{y_i \in N(k)} \left(y_i - \hat{\mu}_y \right)^2. \tag{12}$$

Finally, the relation (5) can be applied. The second reason of imprecision is the fact that the relation (5) refers to the absolute values of the wavelet coefficients, because these values are more translation invariant then their real and

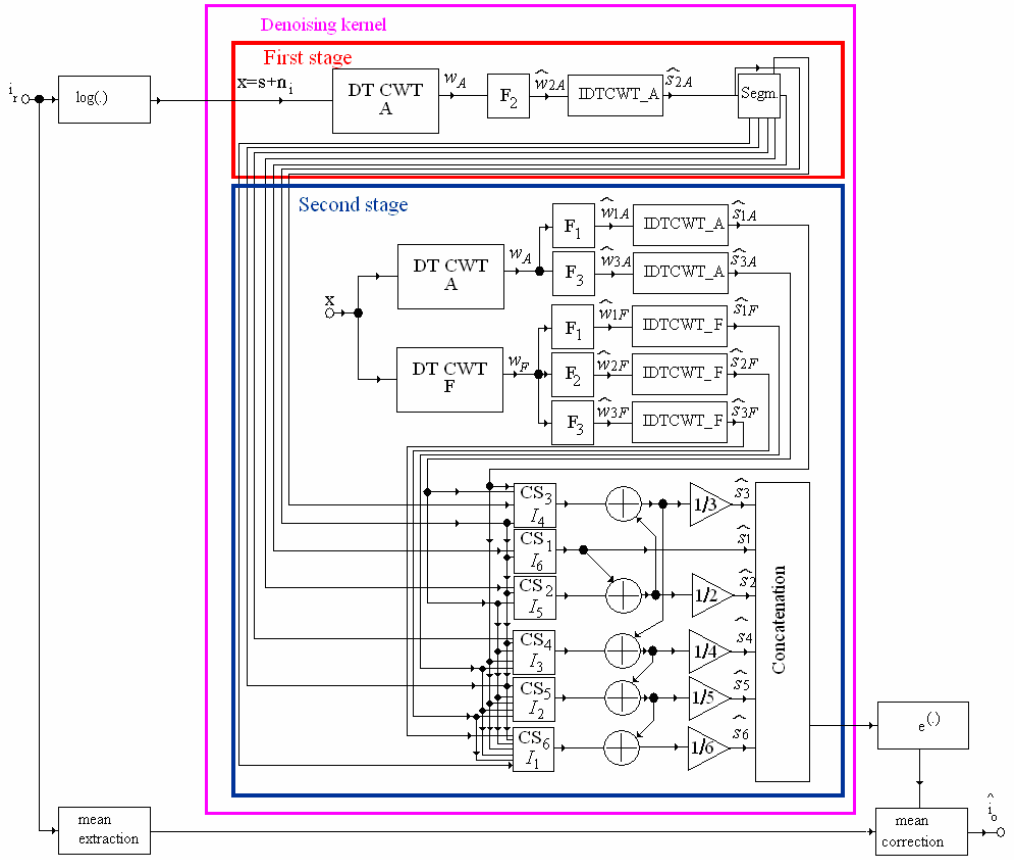

Figure 1. The architecture of the proposed denoising system.

imaginary parts. But the statistical distribution of those real and imaginary parts is supposed to be that described in (1). So, the statistical distribution of the absolute values of the wavelet coefficients can not be of the same type. In the case of the bishrink filter with global estimation of the local variance, the detail wavelet coefficients produced by the first tree of the DT-CWT computation block are indexed with *re* and the detail wavelet coefficients produced by the other tree are indexed with *im*. Applying in order the relations (11), (12) and (5) for the two trees implementing each of the DT-CWT, the local parameters: $_{re}\hat{\mu}_y$, $_{re}\hat{\sigma}_y^2$, $_{re}\hat{\sigma}$, $_{im}\hat{\mu}_y$, $_{im}\hat{\sigma}_y^2$ and $_{im}\hat{\sigma}$ are computed in each neighborhood $N(k)$. Then the global estimation of the marginal standard deviation can be done:

$$\hat{\sigma} = \frac{_{re}\hat{\sigma} + _{im}\hat{\sigma}}{2}. \tag{13}$$

The filter F_3 is the mixed bishrink filter. It was considered for the following reasons. After three iterations of each DWT representing one tree of a DT-CWT, the pdf of wavelet coefficients can be considered Gaussian. In [19] is proposed the mixed bishrink filter. It acts for the first three iterations of each DWT like a bishrink filter with global estimation of local variance, for the fourth iteration it acts as a local adaptive Wiener filter and for the fifth iteration (the last one) it acts as a hard thresholding filter, [5], with the threshold equal with $3\,\hat{\sigma}_n$.

3.2. The Classification

The image $\hat{s}_{2A}$ is segmented in classes which elements have a value of the local variance $\hat{\sigma}_{2A}$, belonging to one of six possible intervals: $I_p = \left(\alpha_p \hat{\sigma}_{2A\max}, \alpha_{p+1}\hat{\sigma}_{2A\max}\right)_{1\le p\le 6}$, where $\alpha_1 = 0$ and $\alpha_7 = 1$. The class selector CS_p in figure 1 selects the class associated to the interval I_{7-p}. For uniform regions $\hat{\sigma}$ is proportional with $\hat{\sigma}_{2A}$. Preliminary tests proved that the six estimates are classified from better to poor in the following sequence: $\hat{s}_{2A}$, $\hat{s}_{3A}$, $\hat{s}_{1A}$, $\hat{s}_{1F}$, $\hat{s}_{2F}$ and $\hat{s}_{3F}$, from the peak signal to noise ratio (PSNR) point of view. These tests also suggest the following values for the bounds of

the intervals I_p: $\alpha_2 = 0.025, \alpha_3 = 0.05, \alpha_4 = 0.075, \alpha_5 = 0.1$ and $\alpha_6 = 0.25$. It is difficult to find a good theoretical explanation for the selection of those bounds because information about the clean image is missing. The proposed algorithm uses only an estimation of the clean image obtained as result of its first stage. We have obtained in preliminary simulations very good denoising results driving this selection procedure with the image of local variances of the clean image but in practice it is not known. The homogeneous zones treatment can be completed by some final adjustments. The results corresponding to the intervals I_1–I_3, $\hat{s}_6$ - $\hat{s}_4$, contain the homogeneous zones. The most homogeneous zones are found in the image that corresponds to the interval I_1. The final adjustments suppose the mean filtering of the results corresponding to the intervals $I_1 - I_3$, using decreasing window sizes 7x7 for $\hat{s}_6$, 5x5 for $\hat{s}_5$ and 3x3 for $\hat{s}_4$. These final adjustments are applied only if the PSNR of the noisy image is inferior to 20 dB.

4. SIMULATION RESULTS

First we have tested the proposed denoising kernel. Second the entire proposed denoising system was analyzed.

4.1. The analysis of the denoising kernel

We compared the proposed denoising kernel to other effective systems in the literature, namely the inter-scale orthonormal wavelet thresholding denoising system proposed in [6] (which comportment in the presence of very noisy images was analyzed), the genuine bishrink filter proposed in [9], (our model), the processor based on the SαS family of distributions presented in [10], the famous BLS-GSM system proposed in [12] (which comportment in the presence of very noisy images was analyzed), and the denoising system based on the estimation of the probability of the presence of a signal of interest proposed in [13]. The comparison was done using for images: Peppers, Lena, Boat and Barbara, all having the same size 512x512 pixels. We have selected these images because each one can be viewed like the prototype of a certain class of images. First we compared the performance in terms of output PSNRs. Next we analyzed the performance obtained in regions with different homogeneity degrees. Let s and $\hat{s}$ denote the clean and the denoised images. The root mean square (rms) of the approximation error is given by: $\varepsilon = \sqrt{\frac{1}{N}\sum_q \left(s_q - \hat{s}_q\right)^2}$, where N is the number of pixels. The PSNR in dB is: $\mathrm{PSNR} = 20\log_{10}\left(\frac{255}{\varepsilon}\right)$. The PSNR values obtained using the denoising systems already mentioned at the beginning of this paragraph are taken from [6], [9], [10], [12] and [13]. For all the test images and all noise levels, with only one exception (Barbara, σ_n=100) the better results are obtained using the BLS-GSM algorithm. This is the effect of three facts: the selection of a very good decomposition, based on the steerable pyramid, having shift invariance and very good directional selectivity; the selection of a very good statistical model, the GSM; and the efficient utilization of the intra-scale and of the inter-scale dependencies of the decomposition's coefficients. The PSNR performance of the proposed denoising algorithm follows closely the performance of the BLS-GSM algorithm. The distance between the performances of these algorithms is of approximately 0.25 dB in the case of the image Lena and of approximately 0.3 dB in the case of the image Barbara, for the levels of noise usually considered in literature, $5<\sigma_n<35$. For the very noisy cases, $35<\sigma_n$, this distance decreases and for the image Barbara when σ_n=100, the output PSNR obtained using the proposed denoising method is higher than the output PSNR obtained using the BLS-GSM algorithm. This comportment can be explained taking into consideration the fact that the image Barbara contains a lot of contours and remembering the very good comportment of the bishrink filter for the contours treatment. In the case of the image Boat the second place is disputed by the algorithm described in [6] and the proposed algorithm. There are two implementation of the algorithm proposed in [10]. The first one, which doesn't make a local estimation, was considered for the treatment of the image Lena. The second implementation makes a local estimation and has better performance. It was considered for the treatment of the image Boat. The classification on the second place of these two algorithms can be explained by the following facts: the superiority of the statistical model of the wavelet coefficients proposed in [10] versus the model proposed in (1); the utilization in both cases of a very good WT, the DT-CWT, having a quasi shift-invariance and a good directional selectivity; the utilization in both cases of effective inter-scale dependence exploitation methods; the utilization of the corrections proposed in this paper; and the qualities of the bishrink filter. Unfortunately, neither the method described in [10] nor the proposed denoising do not exploits the intra-scale dependence of the wavelet coefficients. In the case of images Lena and Barbara, on the fourth place of the classification is situated the denoising algorithm based on the genuine bishrink filter described in [9]. The correction methods proposed in this paper permit to ameliorate the comportment of this denoising system. In the case of the image Boat the forth place is disputed by the

algorithms described in [9] and [13]. Finally, on the last place is situated the algorithm proposed in [6] because it do not exploits any statistical model, it uses the DWT that is not appropriate for the image denoising and it not exploits the intra-scale dependence of the wavelet coefficients. The comparisons already presented take into account only the PSNR, which is a global quality measure. In the following we will present some considerations about the visual quality of the results of some of the mentioned algorithms. First a comparison of the denoising system based on the genuine bishrink filter described in [9] and the proposed denoising algorithm from the homogeneous zones treatment point of view is reported. An objective measure of the homogeneity degree of a region was proposed for synthetic aperture radar (SAR) images and is named enhancement of the equivalent number of looks, (ENL). The ENL of a region is defined by the ratio of the square of the mean of pixels and the variance of the pixels situated in the considered region. The enhancement of the ENL of a denoising method in a homogeneous region is defined like the ratio of the ENLs of the considered region computed after and before the application of the method. We have compared the enhancements of ENL for the proposed denoising method and for the method described in [9] for the images Lena, Boat and Peppers. In each experiment the enhancement of ENL realized by the proposed denoising system is higher then the enhancement of ENL realized by the denoising system based on the genuine bishrink filter described in [9]. To continue the visual quality analysis of the proposed denoising method we have imagined the following procedure. First, the contours of the clean image are detected using the Roberts' detector. Next the contours of the denoising result are detected using the same detector with same parameters. Next the rms of the difference of the two contours images is computed and its dependence on the input PSNR is sketched. For each of the four images the contours treatment realized by the proposed denoising system is better than the contours treatment realized by the system based on the genuine bishrink filter described in [9].

4.2. The analysis of the entire denoising system

First we have analyzed the proposed denoising system on synthetic images. Second we treated some real SONAR images. In [3] was proposed a test image. It was generated concatenating six very different sub-images. The third one is Lena. This is the single from the six sub-images that we have possessed. The entire mosaic was perturbed by the authors of [3] with synthetic speckle noise (multiplicative noise of Rayleigh type) obtaining the test image. We have denoised this test image using some classical despeckling filters and the proposed denoising method. These filters have some specific parameters, like the dimension of the moving window used, or the number of times the filter is applied in the processing of the same input image. The best moving averager for the treatment of the considered noisy image is that having a window of dimensions 5x5. From the family of median filters, the best for our treatment is that which uses a moving window of dimensions 7x7. For the families of Lee's filters, Kuan's filters, Gamma filters and Frost's filters, there are three parameters that can be selected: the dimensions of the moving window, a value called the filter's parameter and the number of times the filter is applied. The best Gamma filter, for the treatment of the considered image, corresponds to the following parameters' values: 5x5, 1.5 and 1. Finally the parameter values of the best Frost's filter are: 5x5, 1 and 1. To appreciate the rms approximation errors of those methods we have extracted the results obtained for Lena, presented in table 1. The smaller rms approximation error is obtained for the proposed denoising method. It is better than the classical despeckling filters. The image presented in the left side of figure 2 is the original SONAR image. It can be seen that the speckle is fully developed. The result obtained, using the proposed denoising method is presented in the right side of figure 2. Analyzing the two images, it can be observed the fact that the noise was practically entirely removed and the fact that the details of the useful part of the input image (textures or edges) were not affected by the treatment proposed. More, some hidden details can be observed in right side of figure 2. An objective measure of the performances of a denoising method for SONAR images is the enhancement of the ENL. The ENLs of the images presented in figure 2 are computed in the same homogenous zone of dimensions 128×128, localized in the left bottom corner. The value obtained for the image in the left side is of 7.34 and the value obtained for the image in the right side is of 76.64. So, the proposed denoising method enhances more than ten times the ENL. Comparing the two images, it can be observed the good conservation of the mean of the useful part of the input image. Of course, the whole treatment can be enhanced if a de-blurring method is also applied. The result from figure 3 was obtained computing four iterations of the DT-CWT. The good quality of the image from figure 2 proves the validity of the theoretical results presented in the previous paragraphs.

Table 1. A comparison of different denoising methods.

Noisy Image	Moving Averager 5	Median Filter 7	Lee's Filter 7-5-1	Kuan's Filter 9-5. 5-1	Gamma Filter 5- 1.5- 1	Frost's Filter 5-1-1	Proposed
3635	571.7	569.8	807.5	732.8	559.5	566	90.6

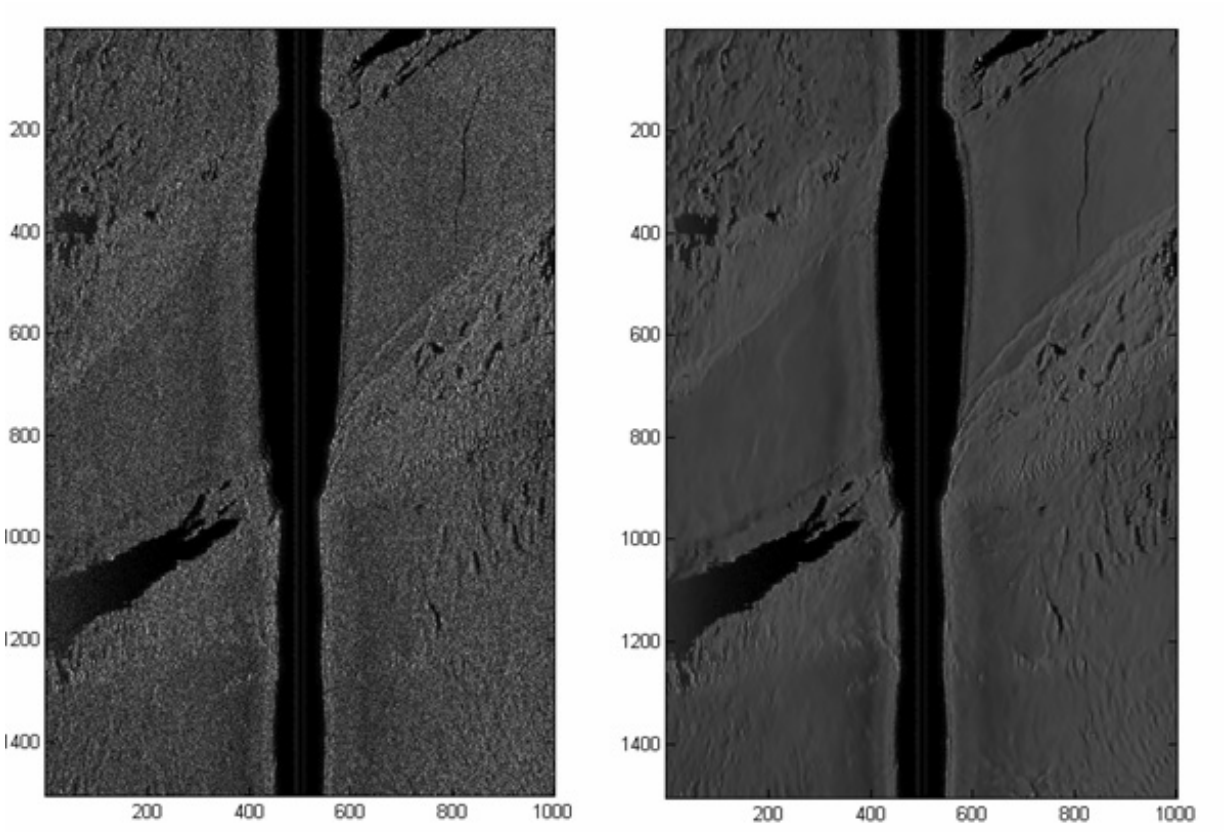

Figure 2. Left-The SONAR image to be denoised, representing a zone of sea floor. The speckle is fully developed. An IFREMER team acquired the image during a campaign on the ocean. The permission to use this image is granted to our research team, Right-The result obtained. The noise was practically entirely removed and the details of the useful part of the input image (textures or edges) were not affected by the treatment proposed. Some hidden details can be observed.

5. CONCLUSION

This paper presents an effective image denoising kernel that optimizes the treatment of homogeneous zones of very noisy images. Our algorithm is inspired from [9] but the diversity enhancement technique proposed can be used also for the improvement of other denoising systems. We presented our simulation results and compared with other published results in order to illustrate the effectiveness of the proposed algorithm. The comparisons suggest that the results of the proposed denoising kernel are competitive with the best wavelet-based results reported in literature, especially for very noisy images. These results encouraged us to use the proposed kernel like the core of a SONAR images denoising system. We evaluated its results on both synthetic data and real SONAR images, validating the theoretical hypotheses used. Due to its performance the proposed denoising method was included in the tool box SONARSCOPE, recently conceived at IFREMER Brest, for the acquisition and treatment of SONAR images obtained by the specialists of this research center during the campaigns on the ocean. One of our future research works will be the inclusion in the proposed algorithm of an effective method to treat the intra-scale dependence of wavelet coefficients. We believe that the idea of directional estimation windows proposed in [16] is a good candidate for this task. Another future research will be dedicated to the search of a good theoretical explanation for the selection of the bounds of the intervals of the segmentation algorithm. Further improvements could be obtained if a better WT and a 3D bishrink filter would be used. This latter avenue is currently under investigation and results will be reported soon.

ACKNOWLEDGMENT

The authors thank Jean Marie Augustin, Ronan Fablet and Xavier Lurton from IFREMER Brest, France for discussions and support.

REFERENCES

[1] Fjørtoft R., Lopès A., Adragna F., "Radiometric and Spatial Aspects of Speckle Filtering", Proc. IGARSS'2000, Honolulu, Hawaii, (2000).

[2] Gagnon L., "Wavelet Filtering of Speckle Noise-Some Numerical Results", Proceedings of the conference Vision Interface 1999, Trois Riviers, Canada, (1999).

[3] Walessa M., Datcu M., "Model-Based Despeckling and Information Extraction from SAR Images", IEEE Trans. on Geosciences and Remote Sensing, 38, 5, 2258-2269 (2000).

[4] Foucher S., Benie G.B., Boucher J.-M., "Multiscale MAP Filtering of SAR images", IEEE Transactions on Image Processing, 10, 1, 49-60, 2001.

[5] Donoho D. L. and Johnstone I. M., "Adapting to unknown smoothness via wavelet shrinkage," J. Amer. Statist. Assoc., vol. 90, no. 432, pp. 1200–1224, Dec. 1995.

[6] Luisier F., Blu T. and Unser M., "A New SURE Approach to Image Denoising: Interscale Orthonormal Wavelet Thresholding", IEEE Transactions On Image Processing, Vol. 16, No. 3 (2007).

[7] Cai Z., Cheng T. H., Lu C. and Subramanian K. R., "Efficient wavelet-based image denoising algorithm", Electronic Letters, 37 (11): 683-685, (2001).

[8] Chang S., Yu B. and Vetterli M., "Adaptive wavelet thresholding for image denoising and compression", IEEE Trans. on Image Processing, 9 (9): 1522-1531 (2000).

[9] Sendur L. and Selesnick I. W., "Bivariate shrinkage with local variance estimation", IEEE Signal Processing Letters, 9 (12): 438-441 (2002).

[10] Achim A. and Kuruoglu E. E., "Image Denoising Using Bivariate α-stable Distributions in the Complex Wavelet Domain", IEEE Signal Processing Letters, 12 (1):17-20 (2005).

[11] Kingsbury N., "Complex Wavelets for Shift Invariant Analysis and Filtering of Signals", Appl. and Comput. Harmonic Analysis10:234-253 (2001).

[12] Portilla J., Strela V., Wainwright M. J. and Simoncelli E. P., "Image denoising using scale mixtures of gaussians in the wavelet domain," IEEE Trans. Image Process., vol. 12, no. 11, 1338–1351 (2003).

[13] Pizurica A. and Philips W., "Estimating the probability of the presence of a signal of interest in multiresolution single-and multiband image denoising," IEEE Trans. Image Process., vol. 15, no. 3, 645–665 (2006).

[14] Ghael S. P., Sayeed A. M., Baraniuk R. G., "Improved Wavelet Denoising via Empirical Wiener Filtering", Proceedings of SPIE, Mathematical Imaging, San Diego, (1997).

[15] Kazubek M., "Improving local Wiener filtering using matched filter", IEEE Proceedings-Vision, Image and Signal Processing, vol. 153, Issue 4, 501-506 (2006).

[16] Shui P.-L., "Image Denoising Algorithm via Doubly Local Wiener Filtering with Directional Windows in Wavelet Domain", IEEE Signal Processing Letters, vol. 12, no. 10, 681-684 (2005).

[17] Coifman R. and Donoho D., "Translation invariant de-noising", Wavelets and Statistics, A. Antoniadis and G. Oppenheim Eds, Springer-Verlag, New York, 125-150 (1995).

[18] Yu T. P. Y., Stoschek A., Donoho D. L., "Translation and Direction Invariant Denoising of 2-D and 3-D Images: Experience and Algorithms", Wavelet Applications in Signal and Image Processing IV, Proceedings SPIE (1996).

[19] Isar A., Isar D. and Quinquis A., "Multi-Scale MAP Denoising of SAR and SAS Images", Sea Technology, 48 (2), 46-48 (2007).

[20] Abdelnour A., Selesnick I. W., "Nearly symmetric orthogonal wavelet basis", Proc. IEEE Int. Conf., Acoust., Speech, Signal Processing (ICASSP), (2001).